Surface structure controlling Nanoparticle behavior:

Magnetism of Ferrihydrite, Magnetite, and Maghemite

Electronic supplementary information

Environmental Science: Nano

Tjisse Hiemstra

Department of Soil Quality, Wageningen University, P.O. Box 47, 6700 AA Wageningen, The Netherlands

Telephone: + 31 317 48 2342

Fax: + 31 317 41 9000

Correspondence to: tjisse.hiemstra@wur.nl

Structure and properties of surface depleted Fh

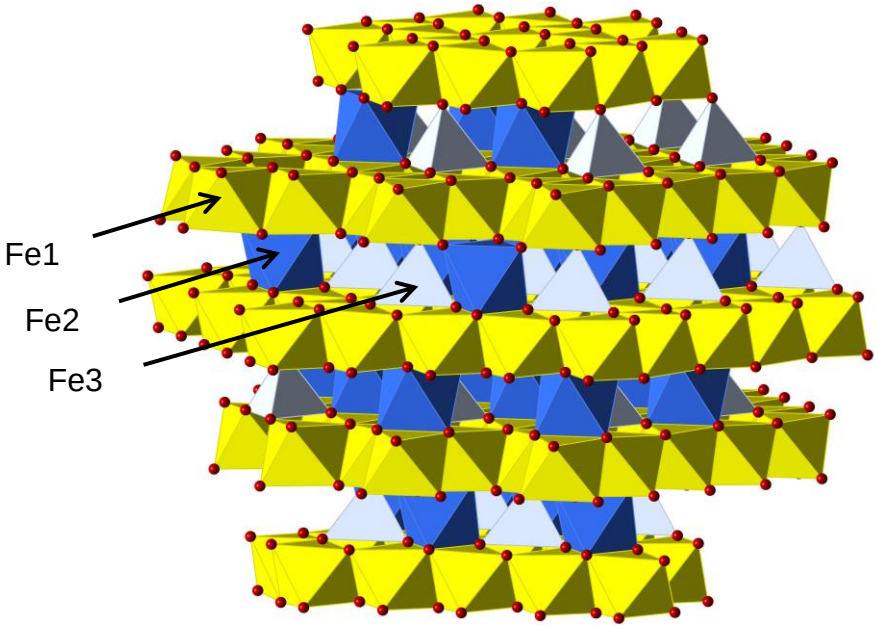

Fig.ESI-1 Representation of the polyhedral structure of a typical Fh particle having a mineral core according to the Fh structure of Michel et al. (Michel et al., 2010) and a surface structure according to the surface depletion (SD) model (Hiemstra, 2013). The particle has three different types of polyhedra, i.e. Fe1-octahedra (yellow), Fe2-octahedra (blue), and Fe3-tetrahedra (light). In the structure, sheets with regular Fe1-octahedra alternate with layers having Fe2-octahedra and Fe3-tetrahedra. In the Fe1 sheet, all octahedra are tightly linked together by a 4- fold Fe1-Fe1 edge-sharing while in the other layer, both types of polyhedra have only Fe2-Fe3 corner sharing on one side. The Fe2 octahedra are highly distorted with three very short (~191 pm) and three very long (~218 pm) Fe-O bonds, which is related to respectively the corner and edge sharing of the Fe2 octahedra with the Fe1 octahedra in the adjacent layers at either side. According to the surface depletion model, the distorted Fe2 octahedra as well as the Fe3 tetrahedra are relatively unstable, particularly when exposed to the surface in hydrated systems. To be present at the surface under these conditions, the ligands of these polyhedra require stabilization by coordination to at least two Fe ions. In other words, these polyhedra will not be present at a hydrated surface while forming singly coordinated ≡FeOH(H) groups. A recent surface structural analysis of Fh (Hiemstra and Zhao, 2016) quantifies the site density of the singly coordinated surface groups (2.8 nm^{-2}) that can form a double corner bidentate complex. All singly coordinated surface groups (3.0 + 2.8 = 5.8 nm^{-2}) may form monodentate innersphere complexes. There are many types of triply coordinated surface groups having a wide range of proton affinities, which leads to internal charge compensation and results in a low effective site density, in the order of ~ 1.4 nm^{-2}. The above particle has 214 Fe^{3+} ions (155 Fe1 + 28 Fe2 + 31 Fe3), 496 O^{2-} ions, and 350 H^{+} ions. The protons are not shown.

Size dependent specific surface area, molar mass, mass density, and number of Fe

The specific surface area A ($m^2\ g^{-1}$) of a spherical particle with a radius d (m) and a mass density ρ ($g\ m^{-3}$) is:

$$A = \frac{6}{\rho_{\text{nano}}\, d} \qquad \text{(ESI 1)}$$

The corresponding mass density ρ_{nano} follows from:

$$\rho_{\text{nano}} = \frac{M_{\text{core}}}{n_{\text{O}} V_{\text{O}}} - \left(\frac{M_{\text{core}}}{n_{\text{O}}} - \text{M}_{\text{H}_2\text{O}}\right)\frac{6}{d}\, N_{\text{H}_2\text{O}} \qquad \text{(ESI 2)}$$

in which M_{core} is the molar mass of the core, n_{O} is the mean number of oxygen ions per metal ion, and V_{O} is the volume of the lattice expressed per mole oxygen ions. The latter is consistent with the mass density at infinite size. The excess density of chemisorbed water due to the presence of surface groups is represented by N_{H2O} and the molar mass of water by $\text{M}_{\text{H}_2\text{O}}$ ($18\ g\ mol^{-1}$).

The corresponding number of Fe ions in the particles (n_{Fe}) follows from:

$$n_{\text{Fe}} = \frac{\rho_{\text{nano}}}{M_{\text{nano}}}\ \frac{\pi d^3}{6}\ \text{N}_{\text{Av}} \qquad \text{(ESI 3)}$$

in which N_{Av} is Avogadro's number and M_{nano} is the overall molar mass of the Fh particle which can be found from:

$$M_{\text{nano}} = (M_{\text{core}} - n_{\text{O}}\, M_{\text{H}_2\text{O}})\ \frac{\rho V_{\text{O}}}{\rho V_{\text{O}} - M_{\text{H}_2\text{O}}} \times \frac{1}{\left(1 - A\, N_{\text{H}_2\text{O}} M_{\text{H}_2\text{O}}\right)} =$$
$$= \frac{M_{\text{core}}}{\left(1 - A\, N_{\text{H}_2\text{O}} M_{\text{H}_2\text{O}}\right)} \qquad \text{(ESI 4)}$$

Note that the factor $1/\left(1 - A\, N_{\text{H}_2\text{O}} M_{\text{H}_2\text{O}}\right)$ in the first part of ESI 4 is accidentally absent in Hiemstra (2015) and Hiemstra and Zhao (2016).

Application

For the various materials studied, the molar mass of the core is M_{core} = 81.65 g/mol Fe for Fh, M_{core} = 79.85 g/mol Fe for γ-Fe_2O_3, and M_{core} = 77.18 g/mol Fe for Fe_3O_4. The mean number of oxygen ions per metal ion is n_O =1.6 for Fh, n_O =1.5 for γ-Fe_2O_3, and n_O = 1.33 for Fe_3O_4. The volume of the lattice expressed per mole oxygen ions is V_O = 10.7 10^{-6} m^3 / mol O for Fh, V_O = 10.4 10^{-6} m^3 / mol O for γ-Fe_2O_3, and V_O = 11.1 10^{-6} m^3 / mol O for Fe_3O_4. The excess water density is N_{H2O} = 12.6 10^{-6} mol m^{-2} for Fh and N_{H2O} = 12.3 10^{-6} mol m^{-2} for γ-Fe_2O_3 and Fe_3O_4.

With the above equations (ESI 1-4), a consistent set of calculations can be done starting with a representative particle diameter d to calculate the mass density ρ_{nano} (ESI 2) and specific surface area A (ESI 1). The value of A can be used to get the corresponding molar mass M_{nano} of the nanoparticle (ESI 4) and this leads to the number of Fe (n_{Fe}) in the particle (ESI 3). The surface area A (m^2 g^{-1}) can also be expressed on a molar basis with A^* in m^2 mol^{-1}.

The above equations can be applied to the Fh particle of Fig.ESI-1. The equivalent spherical diameter is d = 2.57 nm, and the corresponding mass density is ρ = 3.80 10^6 g m^{-3}. The surface area of A = 615 m^2/g. The molar mass is M_{nano} = 94.9 g / mol Fe and n_{Fe} = 214. A^* = 58 10^{+3} m^2/mol Fe.

The OH/Fe neutralization ratio and Protonation of ultra-small Fh clusters

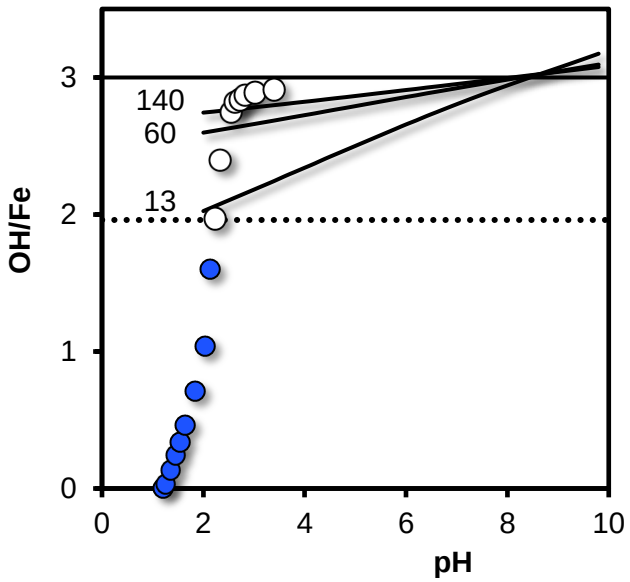

Fig. ESI 2. Relation between OH/Fe ratio and pH in 0.33 M Fe(III) nitrate solutions titrated with 2M KOH (symbols). Data of Collins et al. (2016). Only above OH/Fe ~ 2 (dotted horizontal line), Fh is formed (open symbols). At pH ~ 8, complete neutralization of the system (full horizontal line at OH/Fe=3) is expected since Fh is in its PZC at this pH. A lower OH/Fe ratio is expected if the surface groups of Fh are increasing protonated at lower pH values. The full lines are calculated Fe/OH ratios for Fh as a function of pH in 1 M KNO_3 using the size dependent protonation model of Hiemstra and Zhao (2016). The upper line is for Fh with a mean size of d ~ 2.3 nm. This is the typical value for non-aged freshly prepared 2LFh (Hiemstra and Zhao, 2016). The average number of Fe per particle n_{Fe} =140. The intermediate line is for n_{Fe} = 60 as produced at ultra-fast neutralization (Hiemstra and Zhao, 2016). The lower curve is for nuclei with only n_{Fe} = 13. The OH/Fe ratio of this particle coincides with the experimental OH/Fe ratio where Fh starts to be formed. However, the OH/Fe ratio is an overall value, implying that the actual size of the particles is larger, e.g. equal to the mean size at ultrafast neutralization n_{Fe} ~ 60 (Hiemstra and Zhao, 2016). Larger values may better fit with the relative slow addition of OH in the experiment of Collins et al. (2016) since nuclei are principally very instable and will grow at super saturation. At a ratio OH/Fe ~ 2, particles of ~3 nm are produced at prolonged reaction times (Murphy et al., 1976).

Empirical relation of Fe1 to Fe total and Fe-core of ferrihydrite

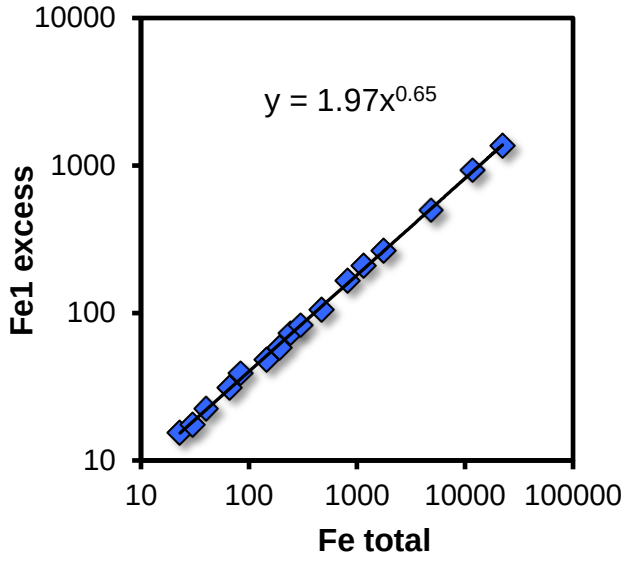

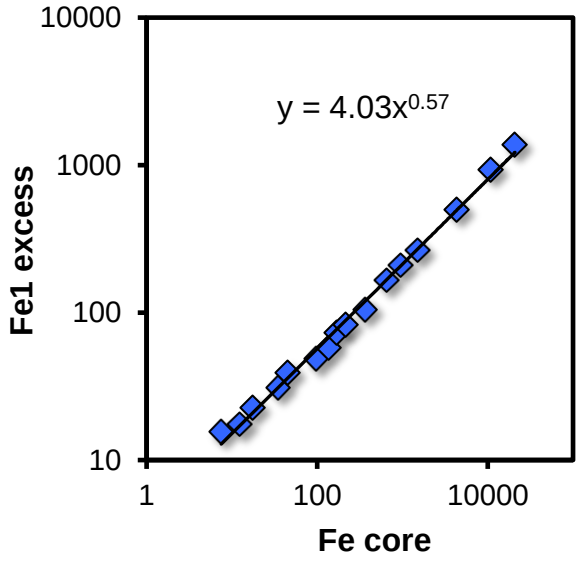

Fig. ESI 3. Relation between total amount of Fe in Fh particles of various size and the amount of Fe1 present (a). Similarly, the relation between Fe in the core of the Fh particles and the amount of Fe1 present in the particles (b).

Scaling total volume to volume based on mean size

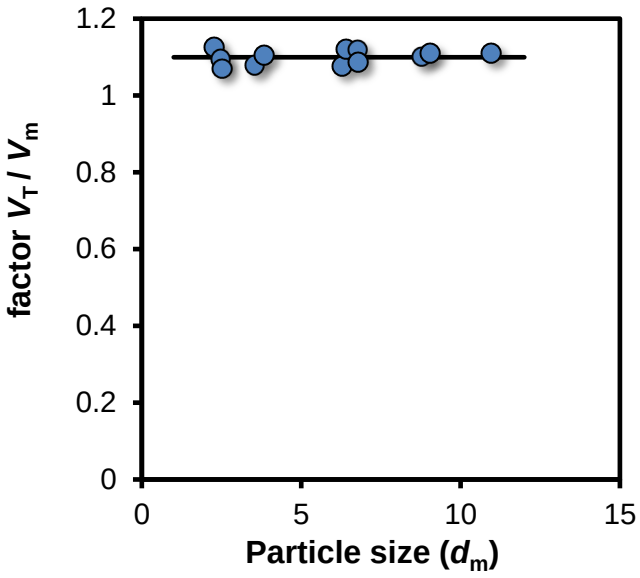

Fig.ESI 4. Volume scaling factor for the difference between the total volume of particles in a distribution and the volume according to the mean size. From the experimental mean size d_m and the standard distribution σ, the frequency f_d of the presence of a particle of certain size d in a Gaussian distribution can be calculated. For each particle i, the volume ($4/3\ \pi\ d_i^{\ 3}$) has been calculated that is summed by weighing for its frequency ($V_T = \Sigma\ f_i\ 4/3\ \pi d_i^{\ 3}$). The total volume V_T is divided by the volume V_m that can be calculated for the experimental mean, leading to the volume factor $f = V_T / V_m$.

Relation between the minimum and mean particle size of Fh upon aging

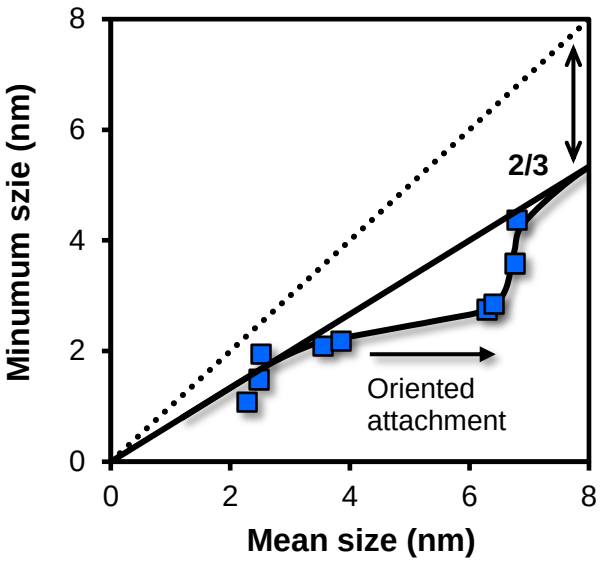

Fig.ESI 5. Relationship between the average and minimum size of Fh particles. The dotted line 1:1 is for monodisperse materials. Fh suspensions are polydisperse, leading to a smaller ratio between the minimum and the average size. For small Fh particles, the ratio is close to 2/3, in agreement with a recent thermodynamic analysis of the stability of Fh in relation to the surface Gibbs free energy (Hiemstra, 2015). For Fh with specific surface area between A = 400-800 m^2/g and an equivalent size of d = 2-4 nm, the solubility of Fh can be well related to the surface Gibbs free energy of Fh if one accounts for polydispersity of the material. The solubility is determined by the smallest particles in the suspension that act as critical nuclei (Hiemstra, 2015). These particles obey the Ostwald-Freundlich equation, while the suspension as a whole apparently obeys the Ostwald equation. Both equations differ by a factor 2/3 (Hiemstra, 2015). When Fh particles have reached a size near ~ 4 nm (A ~ 400 m^2/g) by aging, the mean size quickly increases (Fig. 6 main text) in contrast to the minimum size. This leads to a significant deviation from 2/3 ratio. This can be explained by assuming oriented attachment of particles forming doublets. At prolonged aging, the suspension returns to the 2/3 ratio between the minimum and average size.

Surface energetics of ferrimagnetic and antiferromagnetic Fh

Based on thermochemical data (Majzlan et al., 2004), a relation between enthalpy of dissolution (J mol^{-1}) and the specific surface area (m^2 mol^{-1}) can be established (Hiemstra 2015), resulting in a surface enthalpy of ΔH_{surf} = 0.096 J m^{-2} and an enthalpy of (oxo) formation of the virtual bulk of $H^o_{f,ox}$ = -405.2 ± 1.2 kJ/mol $FeO_{3/2}$. The latter value refers to Fh as a hypothetical Fe oxide and therefore, it is expressed per mole $FeO_{3/2}$. It can be back-calculated to any other chemical composition that is enriched with hydroxyls or water using a hydration reaction, e.g. 10 $FeO_{3/2}$ (s) + H_2O(l) ⇔ $Fe_{10}O_{14}(OH)_2$ (s).

The above enthalpy of formation $H^o_{f,ox}$ is based on experimental information and was found to be close to the enthalpy of formation calculated by Pinney et al. (2009) using first principle computations, giving $H^o_{f,ox}$ = -406.7 ± 1.5 J mol $FeO_{3/2}$. The mean value of both approaches was used to establish the surface enthalpy ΔH_{surf} leading to a slightly higher value of ΔH_{surf} = 0.107 ± 0.01 J m^{-2} than calculated with the experimental data only.

Since the computational value of $H^o_{f,ox}$ refers to the most stable form of Fh, i.e. ferrimagnetic Fh (Pinney et al., 2009) and the experimental thermochemical data are most probably for antiferromagnetic Fh, the surface enthalpy of antiferromagnetic Fh may be ΔH_{surf} = 0.096 J m^{-2} rather than ΔH_{surf} = 0.107 J m^{-2}. It will lower the surface Gibbs free energy for antiferromagnetic Fh to about ΔG_{surf} = 0.175 J m^{-2}.

Based on an energy difference of ~1 kJ/mol between antiferromagnetic Fh and ferrimagnetic Fh, the surface Gibbs free energy will then be ~0.029 J m^{-2} higher for ferrimagnetic Fh (See Fig.ESI 6), i.e. ΔG_{surf} = 0.204 J m^{-2}. In case of a Gibbs free energy difference of ~0.6 kJ/mol (Larrucea et al., 2014), ΔG_{surf} = 0.192 J m^{-2}.

Relation surface Gibbs free energy and lattice stability

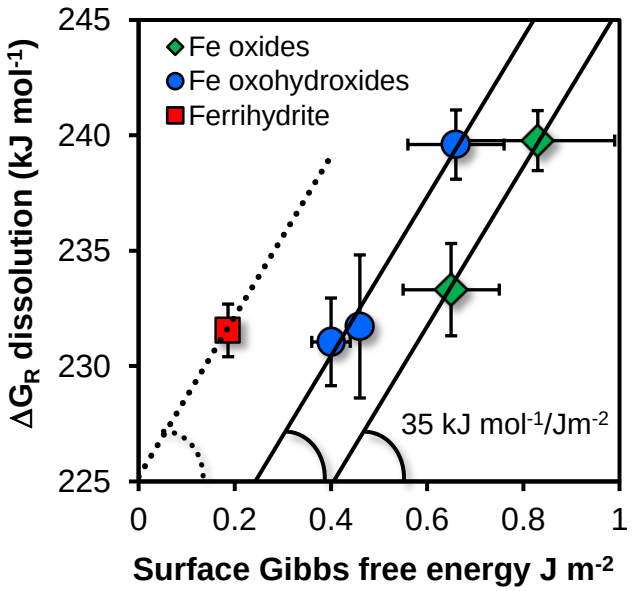

Fig. ESI 6. Relation between the Gibbs free energy of surface formation (J m^{-2}) and the Gibbs free energy of dissolution of Fe (hydr)oxides (kJ/mol $FeO_{3/2}$), according to the reaction $FeO_{3/2}(s) + 3/2\ H_2O(l) \Leftrightarrow Fe^{3+}(aq) + 3\ OH^-(aq)$. The Fe oxohydroxides (spheres) and Fe oxides (diamonds) differ in the mean coordination number, being respectively CN = 3 and CN = 4. Data from Hiemstra (2015). The corresponding slope of the relationships is 35 ± 0.7 kJ mol^{-1} per J m^{-2} and the inverse value is 0.0284 ± 0.006 J m^{-2} per kJ mol^{-1}. Application to Fh (red square) enables the calculation of the change in surface Gibbs free energy in case of a Gibbs free energy difference in relation to difference in stability of the different magnetic states of Fh. This leads to the prediction of the crossover point in the chemical stability of antiferromagnetic and ferrimagnetic Fh.

Influence of added ligands on magnetization of Fh

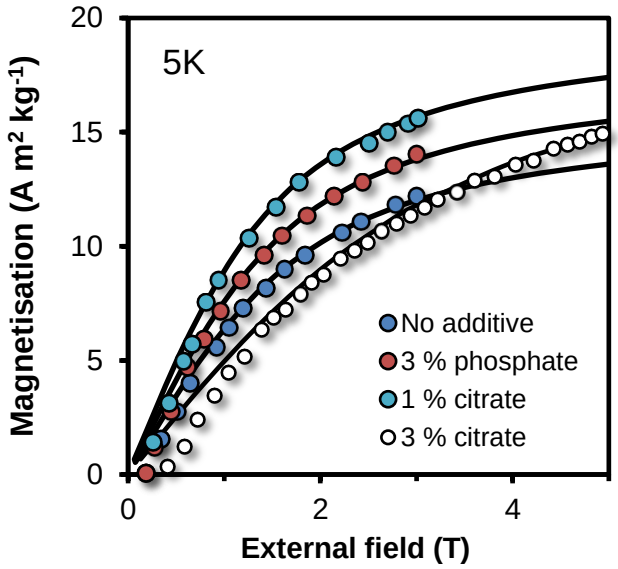

Fig.ESI 7. Magnetization curves of Fh aged during 50 days at 50 ^{o}C (Water activity = 1) without additives or with 3 % phosphate or 1 % citrate (Data of Cabello et al. (2009)) in comparison to the Fh (3 molar % citrate) at zero time aging (Data of Michel et al. (2010)). The lines have been calculated using the Langevin expression, yielding for the data of Cabello et al. (2009) fitted maxima of respectively M_s = 16, 18, and 20 A m^2 kg^{-1}. For the calculation of the curve of Michel et al. (2009), their reported value for M_s (M_s = 20.8 m^2 kg^{-1}) has been used. Although similar maxima are found when citrate is used, the magnetization curves are very different. All samples show coercivity, but it is largest in the non-aged Fh sample of Michel et al. (2010).

Stability increase of ferrimagnetic Fh at decrease of surface Gibbs free energy

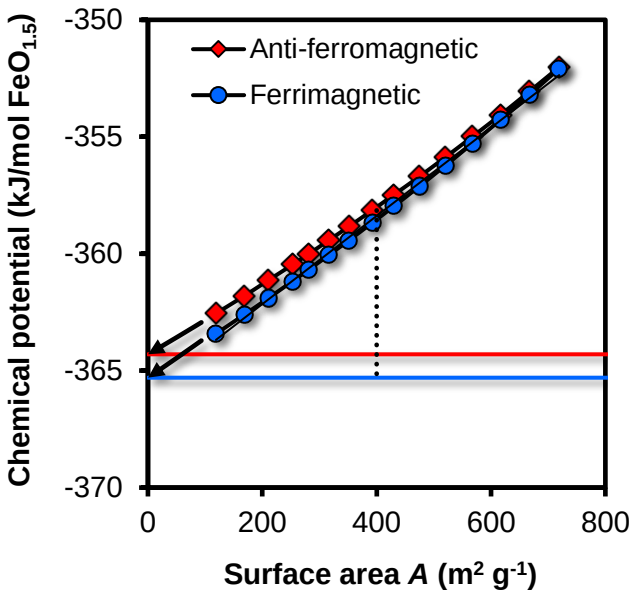

Fig.ESI 8. Chemical potential of antiferromagnetic Fh (red diamonds) and ferrimagnetic Fh (blue spheres) as a function of the specific surface area, covering the size range d ~ 2 - 11 nm. The chemical (oxo) potential of the virtual bulk material of ferrimagnetic Fh is G^{o}_{bulk}= -365.3 kJ/mol $FeO_{3/2}$ (blue horizontal line). For antiferromagnetic bulk Fh, the enthalpy is ~ 1 kJ higher (red horizontal line). The size dependency of the chemical potential of Fh particles is due to the variable contribution of surface Gibbs free energy (γ_{surf}). For antiferromagnetic Fh, γ_{surf} = 0.175 J/m^2 is used. For ferrimagnetic Fh, the surface Gibbs free energy is lowered from γ_{surf} = 0.204 J m^{-2} by 0.015 J/m^2 to ΔG_{surf} = 0.189 J/m^2. This lowering of ΔG_{surf} is for instance due to the presence of adsorbed citrate, that will lead to a shift of the crossover point making ferrimagnetic Fh chemically stable over the entire particle size range compared to anti-ferromagnetic Fh in systems without adsorbed ions.

REFERENCES

Cabello, E., Morales, M.P., Serna, C.J., Barron, V. and Torrent, J. (2009) MAGNETIC ENHANCEMENT DURING THE CRYSTALLIZATION OF FERRIHYDRITE AT 25 AND 50 degrees C. Clays Clay Min. 57, 46-53.

Collins, R.N., Rosso, K.M., Rose, A.L., Glover, C.J. and Waite, T.D. (2016) An in situ XAS study of ferric iron hydrolysis and precipitation in the presence of perchlorate, nitrate, chloride and sulfate. Geochim. Cosmochim. Acta 177, 150-169.

Hiemstra, T. (2013) Surface and mineral structure of ferrihydrite. Geochim. Cosmochim. Acta 10, 316–325.

Hiemstra, T. (2015) Formation, stability, and solubility of metal oxide nanoparticles: Surface entropy, enthalpy, and free energy of ferrihydrite. Geochim. Cosmochim. Acta 158, 179–198.

Hiemstra, T. and Zhao, W. (2016) Reactivity of ferrihydrite and ferritin in relation to surface structure, size, and nanoparticle formation studied for phosphate and arsenate. Environmental Science-Nano 3, 1265-1279.

Larrucea, J., Lid, S. and Ciacchi, L.C. (2014) Parametrization of a classical force field for iron oxyhydroxide/water interfaces based on Density Functional Theory calculations. Computational Materials Science 92, 343-352.

Majzlan, J., Navrotsky, A. and Schwertmann, U. (2004) Thermodynamics of iron oxides: Part III. Enthalpies of formation and stability of ferrihydrite (similar to Fe(OH)(3)), schwertmannite (similar to FeO(OH)(3/4)(SO4)(1/8)), and epsilon-Fe2O3. Geochim. Cosmochim. Acta 68, 1049-1059.

Michel, F.M., Barron, V., Torrent, J., Morales, M.P., Serna, C.J., Boily, J.F., Liu, Q.S., Ambrosini, A., Cismasu, A.C. and Brown, G.E. (2010) Ordered ferrimagnetic form of ferrihydrite reveals links among structure, composition, and magnetism. Proceedings of the National Academy of Sciences of the United States of America 107, 2787-2792.

Murphy, P.J., Posner, A.M. and Quirk, J.P. (1976) Characterization of Partially Neutralized Ferric Nitrate Solutions. J. Colloid Interf. Sci. 56, 270-283.

Pinney, N., Kubicki, J.D., Middlemiss, D.S., Grey, C.P. and Morgan, D. (2009) Density Functional Theory Study of Ferrihydrite and Related Fe-Oxyhydroxides. Chemistry of Materials 21, 5727-5742.